
Article:
Palmer, J.W., Ghadbeigi, H. orcid.org/0000-0001-6507-2353, Curtis, D. orcid.org/0000-0001-6402-6996 et al. (1 more author) (2018) An experimental study of the effects of dressing parameters on the topography of grinding wheels during roller dressing. Journal of Manufacturing Processes, 31. pp. 348-355. ISSN 1526-6125

https://doi.org/10.1016/j.jmapro.2017.11.025

An Experimental Study of the Effects of Dressing Parameters on the Topography of Grinding Wheels during Roller Dressing

Abstract

Vitreous-bonded grinding wheels are widely used for machining features on aerospace components achieving high material removal rates under high pressure coolant. Dressing is a vital stage in the grinding process to ensure a consistent wheel topography and performance. However, the effects of roller dressing on functional performance of vitreous grinding wheels as well as its influence on different abrasive grit morphologies have not been fully characterised. This paper studies the influence of dressing parameters on the topography, morphology and characteristics of the surface of different vitrified abrasive wheels in order to better understand the process and therefore optimise the preparation of grinding wheels for industrial machining. Alumina grinding wheels with conventional and engineered grit shapes were dressed at two different infeed rates over a range of seven different speed ratios (from -0.8 to +1). An experimental methodology has been developed incorporating a range of known techniques to define the abrasive wheel condition including measured power consumption and ground graphite coupons as well as using optical microscopes to measure grain fracture flats, peak density and abrasive grain shape. It has been found that power consumption of the grinding wheel spindle increases at higher infeed rates and speed ratios. This leads to increased fracturing of the grains and whole-grain pull out. According to the results the infeed rate has a more substantial effect on wheel topography than speed ratio and the response of engineered grit morphologies to dressing is dependent on grit orientation.

Keywords: Dressing; Grinding; Topography;

1.0 Introduction

Grinding is a widely used machining process utilised for both high material removal roughing processes as well as high quality finishing operations. A vital stage in this process is wheel preparation whereby the grinding wheel is prepared for cutting by truing (to remove wheel run-out), dressing (to sharpen abrasive grains) and forming (to generate a particular shape in the wheel)[1]. Dressing is also used to remove any loaded or built-up workpiece material deposited on the wheel surface.

The dressing process can be performed in a number of ways including traditional techniques of single point and roller dressing, as well as more recent methods such as Electrolytic in-process dressing (ELID) and Laser[2]. Saad et al.[3], who examined both point and roller dressing, highlighted the influence of overlap ratio on component surface finish. For this investigation roller dressing was studied due to its common use in industry when form grinding for aerospace component applications.

Roller dressers consist of a cylindrical body with a single layer of diamond particles impregnated in a metal matrix. Dressing rolls can also be made to specific forms which will then be generated in the

surface of the abrasive wheel, therefore enabling the grinding of complex features onto the workpiece [4]. This leads to a much faster dressing process and longer lifetime for the dresser in complex feature grinding compared with a single point method [5].

There are three key variables that affect the dressing operation including infeed rate, rotational direction and speed ratio [2]. The effect of each of these was investigated.

- Infeed rate - the rate at which the dresser moves normal to the circumference of the wheel.
- Rotational direction - describes the direction the dresser turns relative to the wheel, synchronous (wheel and dresser spin in opposite directions, the angular velocity of the dresser over the wheel is negative) and asynchronous (wheel and dresser spin in the same direction, the angular velocity of the dresser over the wheel is positive).
- Speed ratio (q_d) - the relative surface speed of the dresser to the surface speed of the abrasive wheel.

Although the mechanics and simulation of single point dressing is relatively well covered [4], [6]–[8], there is a less knowledge about the mechanisms involved in roller dressing and its influence on the topography of vitreous grinding wheels. It is well known that crush dressing occurs at high positive speed ratios (q_s =1) i.e. the dresser and grinding wheel surface speeds are equal. This is the only active mechanism that causes grain fracture at the surface of the wheel and generates a fresh topography on the cutting edge. In this condition the wheel and dresser are subjected to a high normal force due to the wheel/roller pressing into one another with little abrasive removed by cutting [1].

Malkin and Murray [9] have found that in rotary dressing of aluminium oxide grinding wheels the vertical and horizontal force components peak when the speed ratio is at unity. They also demonstrated that specific dressing energy reduces by an increase of the infeed rate. SEM imaging suggested that the interference angle of the dresser on the abrasive wheel will influence dressing specific energy. Interference angle was defined as the angle of the trochoidal path of the diamond relative to the surface of the abrasive wheel and it can be altered by the infeed rate [9].

Several models have been developed to simulate grinding wheel behaviour during dressing. This includes considering it as a tribological system and calculating the ideal engagement volume of a dresser diamond against the abrasive wheel. Linke [10] used this to understand the influence of speed ratio on the normal force and acoustic emission output when dressing. When dressing at unity, the normal forces were high and caused shattering of the grinding layer through whole grains breaking off the surface. A Finite Element Modelling (FEM) study followed treating the wheel as a homogenous body and creating a two-dimensional model based on the linear elastic stress state. The results indicated that previous dressing strokes can weaken the abrasive wheel bond and result in high wheel wear directly after dressing, this effect was observed even after a ‘finishing’ dressing stroke [11]. Saad [3] compared two different empirical surface roughness models to understand the impact of dressing parameters on workpiece surface integrity. This showed the influence of interference angle on component quality. A good summary of grinding wheel topography models is given by Doman et al. [12] which highlighted that the mechanics of dressing has not been studied in great detail.

It is well known that the performance of a grinding wheel during cutting is directly linked to wheel topography [13]. As dresser interaction with the grinding wheel influences the wheel cutting surface, topography therefore can be used as a measure of dressing effectiveness. To measure the response of the grinding wheel to different dressing parameters, a robust technique must be identified to capture its topography. Different contact and non-contact based systems have been used in literature including Backer et al. [14] who used a soot-track method. A wheel was rolled on a glass plate coated with carbon-black to determine the number of contacting grains per area as soot would be removed where the grains contacted the glass. Although indicating possible active grains this method gives no information on the shape of the cutting edges. To conquer this many papers have utilised a stylus technique [15]–[18] including Butler and Blunt [19] who used 3D stylus profilometry to determine density of summits, summit curvature and root-mean-square roughness.

Research has also been conducted using image processing methods to assess wear and fracture on abrasive wheels. Lachance et al. [20] introduced a technique to identify wear flat area using charge coupled device camera images of a grinding wheel and LabView image processing software. Arunachalam and Ramamoorthy [21] as well as Yasui et al. [22] completed similar work determining flat regions on abrasive grits. Application of replica techniques has also been investigated by Bhaduri et al. [23] who used both graphite and resin compound to obtain positive and negative profiles of the wheel. Summit density was determined from this as well as average roughness by using a Form Talysurf stylus on the positive profiles. Cai and Rowe [18] also used resin replicant to measure cutting edge density and cutting edge dullness of four different Cubic Boron Nitride (CBN) wheels. This proved that resin replicas are best measured under optical interferometry.

To the best knowledge of the authors, the literature is limited on the effect of roll dressing on characteristics of vitreous grinding wheel topographies, especially the influence of different abrasive grit morphologies (wheels with engineered grains). This work aims to develop the fundamental understanding of the process and define the effect of abrasive grit morphology on the response of a grinding wheel to different roller dressing parameters including infeed rate, rotational direction and speed ratio.

2.0 Experimental Framework

Three different alumina grit wheels (as indicated by wheels A, B and C in Figure 1) with a fine, #80 mesh, grit size, a medium porosity and manufacturers hardness grade H were tested over seven different speed ratios (-0.8, -0.6, -0.4, 0.4, 0.6, 0.8, 1) and two infeed rates (0.002 mm/rev and 0.0005 mm/rev) using a flat roller dresser. A full, random factorial Design of Experiment with a full set of repeats was used to determine the test order.

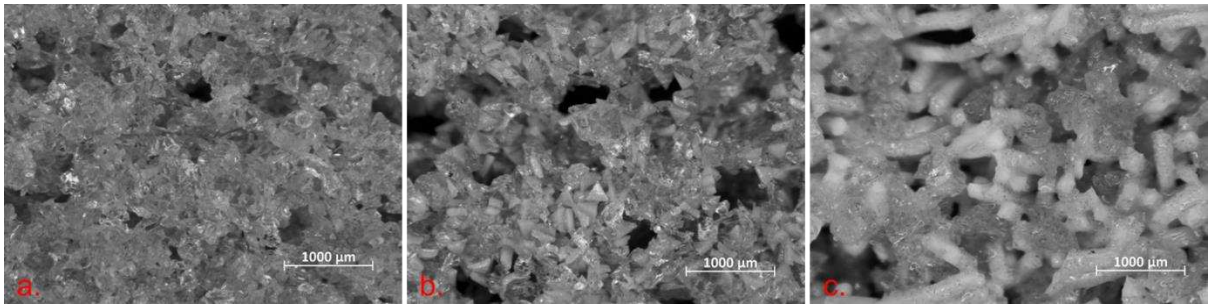

Figure 1 – Micrographs of the three different wheels tested with varying morphology (a) wheel A with conventional grits (b) wheel B containing triangular grits and (c) wheel C containing elongated grits.

The as received grinding wheels were dressed prior to the experiments to true and dress the wheel surface to a controlled parameter set to remove the influence of variation in wheel manufacture processes. A second dress was performed with a total dress depth of 0.3 mm and power during dressing was measured. The total dress volume was constant for each dressing condition. The background power conditions where the spindle was in free rotation at speed (not in contact) was also measured and net power consumption of the grinding spindle was calculated as power during dressing minus background power conditions. A Load Control Incorporated Power Monitoring kit (4-20mA output) with a National Instruments 9201 DAQ box was used to capture the data at a sampling rate of 20 kHz. Each recorded reading was an average 1000 data points. A single grinding pass (1200mm/min feed rate, 50 m/s wheel speed) on a graphite coupon (Grade GD4430) was performed after dressing to measure the 'average' wheel 2D surface profile topography. The surface roughness of the graphite coupon was then measured in the lay direction (perpendicular to the feed direction),

which is representative of the average surface topography across the grinding wheel width, using a portable roughness probe. Measurements used ISO1997 standard with a 5N applied probe force and evaluation length of 4.0mm together with a cut-off wavelength (λs) set at 0.8mm. To ensure the statistical validity of the results the measurements were repeated five times for each coupon and the average surface roughness, Ra, was calculated. The area surface topography of the grinding wheel was further investigated using different techniques explained in Section 2.1.

All dressing trials were conducted on a Makino A100 universal horizontal machining centre using the 5-axis VIPER grinding capability and standard Hocut 768 coolant (at a percentage of 6-8% and a pH of 8.5-9.5). The dresser spindle was directly driven with 11kW max power, 8000rpm max speed, torque of 14Nm and continuous dressing capability.

2.1 Wheel Topography Analysis

An optical focus variation microscope (Alicona InfiniteFocusSL) was used to characterise the grinding wheel topography. Due to the restricted working distance, the outer (cutting) wheel edge could not be measured directly under the microscope. Therefore a two-part silicon rubber replicate material (Struers Repliset T3) was deposited in the middle of the cutting surface of the wheel to take a replica of the topography. A 3D printed jig was used to ensure a constant volume of Repliset was applied at 3 different locations on the wheels circumference (Figure 2). After curing the replica, samples were scanned under an optical focus variation microscope (Alicona InfiniteFocusSL). Vertical and lateral resolutions of 1µm and 10µm respectively were used over a 5.7mm^2 area at x100 magnification. This generates a distribution of heights (z axis) histogram, over the scan area, which is then plotted as a cumulative frequency graph. Figure 3 shows the frequency graph generated, the negative region being valleys on the replica (which are peaks on the wheel). The gradient of this region of the graph indicates the average grit shape as the shallower the gradient, the less the increase in area with distance into the replica so the sharper the abrasive grits.

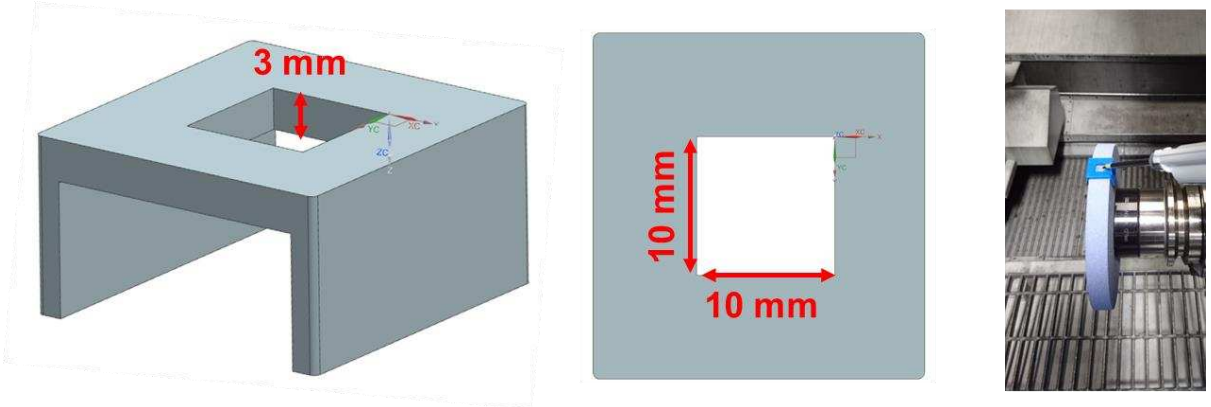

Figure 2 – Dimensions of the 3D printed jigs for application of the replicant which were placed at 3 different points on the grinding wheel.

Any peak on the surface can be considered as a single tip of a cutting grit where , ‘a peak is defined as a point in the data array which is higher than its eight nearest neighbours’[15]. Equation 1, defined by Butler et al. [19], was used to reduce the lateral spacing in the scan to 66µm to ensure only whole grits were considered as peaks (not micro peaks on the grain surface). This facilitates identifying any loss of whole abrasive grains from the cutting surface of the wheel (whole grain pull out), a key mechanism in wheel breakdown [2]. It is also very difficult to accurately determine active micro peaks on abrasive grains so simplifying cutting points to single grains provides a better representation of the abrasive wheel surface. The average grain size is denoted as d_g and SS_{opt} is the optimum sample spacing. A Matlab program was developed, according to the criteria introduced by Butler, to identify the number of peaks from the reduced scan dataset.

$$d_g/4 \leq SS_{opt} \leq d_g/3 \qquad \textbf{Equation 1}$$

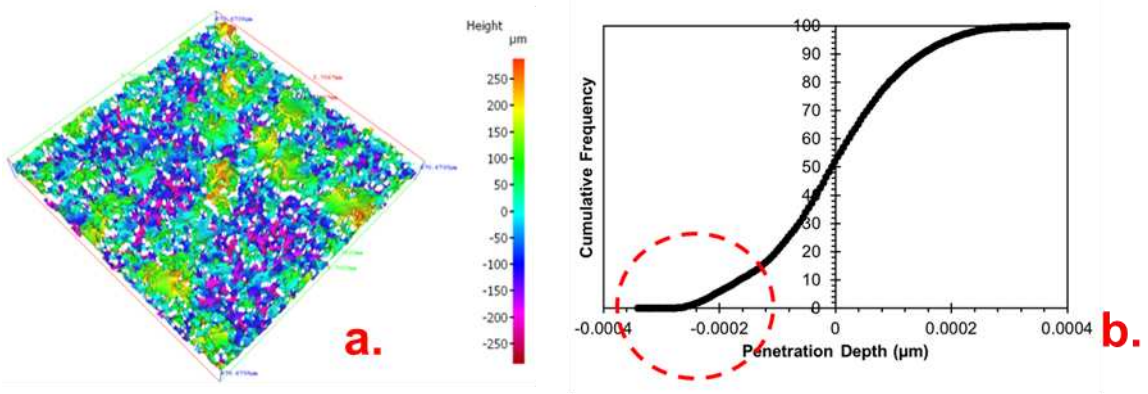

Figure 3 – (a) High resolution Alicona scan of wheel replica (b) Cumulative frequency graph plotted from the histogram of different heights generated by the Alicona microscope scan. The circle identifies the region of interest, the gradient of which indicates grit shape.

The wheel was also examined under a Zeiss Discovery V8 optical microscope, at x10 magnification, using an incident light source perpendicular to the wheel surface. This provides information about the fracture behaviour of the grits similar to those reported by Hwang et al. [24], [25]. Considering the fact that reflection of the incident light is much higher from flat regions on the grits they therefore appear as bright spots on the image. Six different grain flats were visually identified across high magnification optical images and a threshold value defined based on the calculated average intensity of the grayscale pattern for the selected grain flat (Figure 4). A Matlab program was developed to identify the number of pixels above the calculated threshold intensity for each wheel image. Images were taken at three different locations on the wheel circumference after every test, thus indicating the average percentage of flat regions generated on the wheel surface. The fracture mechanisms of the grits were also investigated through the post-dressing analysis of small sections of the wheels. These wheel pieces were broken and gold coated to take SEM micrographs of the abrasive grits at the cutting surface using a high resolution FEG-SEM.

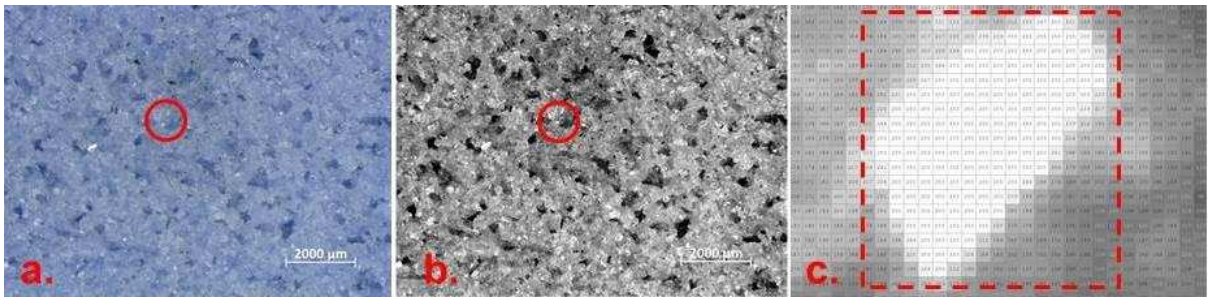

Figure 4 – Fracture flat threshold intensity calculation (a) identification of the flat (b) conversion of the image to grayscale (c) the pixel region around the flat from which the average intensity is calculated.

Figure 5 shows a flow diagram detailing the complete analysis conducted for each dressing condition. Dresser wear was assumed to be minimal as a fresh, flat dresser was used for the investigation. In industry the same dresser design used under the dressing conditions tested in this work has a lifetime well beyond the total dressing volume in the experimental trial [ref personal correspondence]. The whole experimental investigation was repeated also so variation between repeats can be observed to determine if substantial dresser wear is occurring.

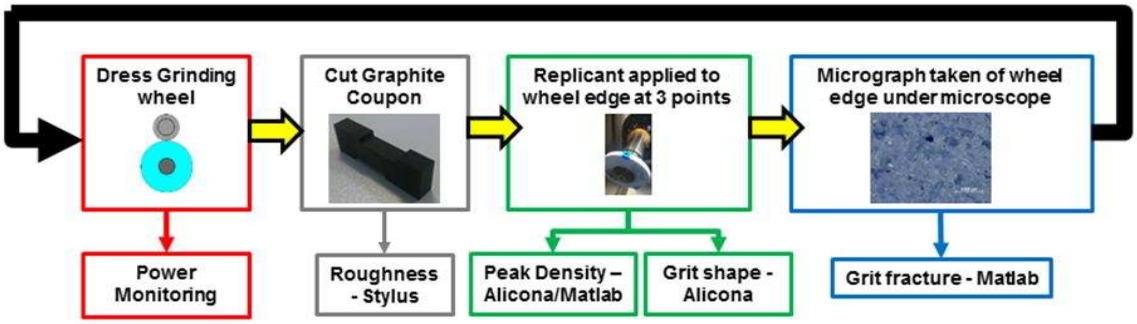

Figure 5 – Process flow diagram for the complete analysis process.

3.0 Results and Discussion

The results shown in Figure 6 are the net power consumption of the grinding spindle plotted as a function of the dressing speed ratio for three different abrasive wheels of varying grit morphology (wheel A, B and C).

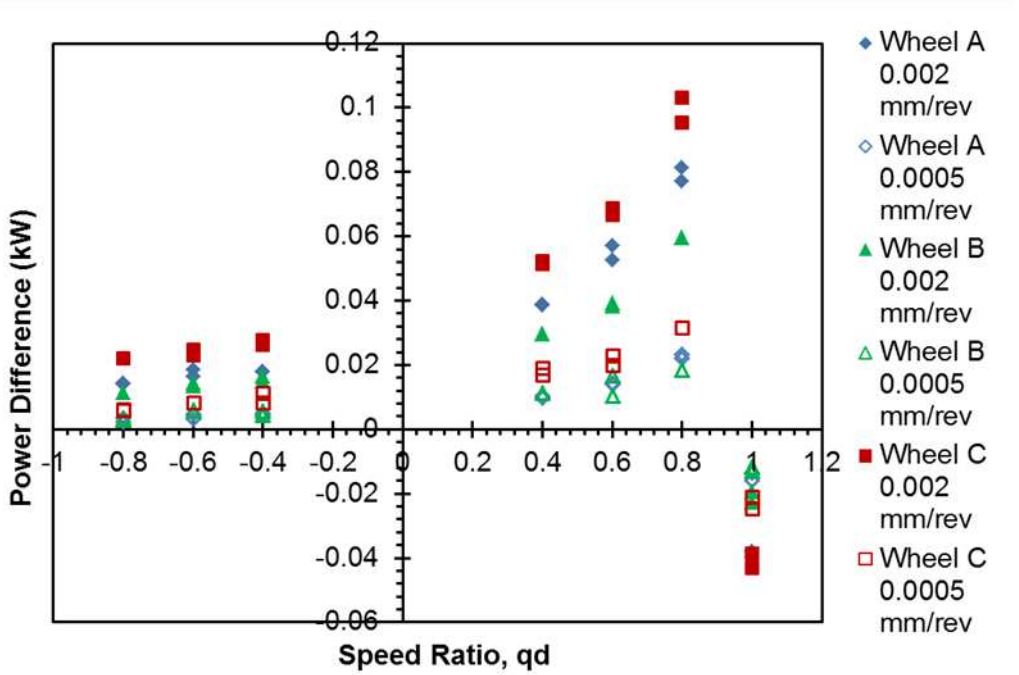

Figure 6 – The average power consumption difference between before and during dressing.

According to Figure 6 the power difference changes very sharply for all the wheels at positive speed ratios (synchronous region) using high infeed rates. This could be due to the presence of large interference angles as it is reported that at high interference angles the dresser forces are greater, therefore power consumption is expected to rise as the relative dresser/wheel impact speeds increase [3]. Figure 6 also shows that the consumed power dramatically decreases (negative power difference) at the speed ratio of unity where the dresser roll assisted the grinding wheel in its rotation due to their equal surface speeds.

Wheel C, with the elongated grain structure, was found to have the highest power consumption during dressing, followed by conventional grit (wheel A) and combined triangular and conventional grains (wheel B). This is likely due to the much larger size (approx. 5 times) of elongated grains compared to the other morphologies, meaning greater amounts of the hard Alumina grains to be fractured by the diamond of the roller dresser. Moreover, due to the relatively extreme aspect ratio (longest dimension

over smallest dimension of an individual abrasive grit) of the wheel C elongated grits, compared to the other morphologies (approx. 5 times larger), grit orientation will have a much more significant impact on grain fracture.

SEM images of the sample wheel sections, Figure 7, show that grit fracturing can occur in multiple orientation, for wheel A, for any interference angle. However, in wheel C, with large aspect ratio of the grits, grains facing out of the wheel will fracture at a very different force than those lying flat on the surface. It is expected that increased fracturing will be seen in grains protruding out of the surface of the wheel as they have less support from the bond and other grains when impacted by a dresser diamond. As for wheel B, this showed the lowest power consumption as the grits indicated levels of microfracturing on the tips of the triangles, suggesting dresser energy was imparted to the microchips and reducing the power required for fracture.

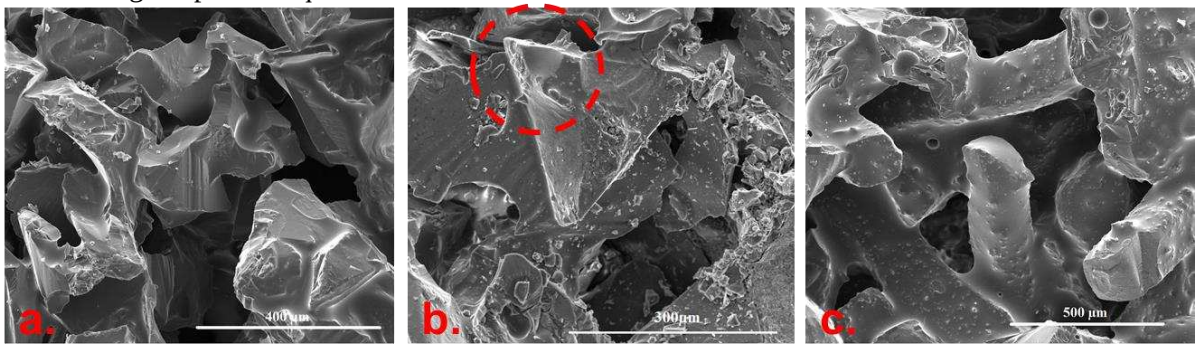

Figure 7 – (a) Shear fracturing of conventional abrasive grits (wheel A) (b) microfracturing of triangular grain tips (wheel B, fractured tip circled) (c) variation in aspect ratio of elongated grains causing different fracture behaviour (wheel C).

Figure 8a shows the measured average roughness parameter (Ra) for the graphite coupons after each dressing process. The graph shows that at very negative and positive power difference, corresponding to high infeed rate and speed ratio, the surface roughness increases. This high deviation of the graphite surface indicates higher variation in the topography of the abrasive wheel, generated due to steep interference angles and high velocity impacts between the dresser diamonds and the wheel abrasive grits. This causes extensive fracturing of the bond and abrasive which results in a highly variable wheel topography. Therefore when the dressing power consumption is higher the wheel topography consists of an 'open' structure with a topography that is dominated by sharp cutting points (peaks) with large spacing between them (valleys). This is because for higher speed ratios the impact forces between the abrasive and diamond will be greater due to the faster rotational speed, and therefore higher impact speed, of the wheel and the roller dresser. As the speed ratio reaches unity, then the only active dressing mechanism would be crush dressing that removes material from the wheel, so the fracture mechanism becomes dependent on compressive stress from the dressing roller. Crush dressing generates the most aggressive surface, as also noted by Malkin and Murray [5], [26]. The difference between high and low infeed rates is more noticeable in synchronous dressing than asynchronous. In synchronous dressing the interference angle is much steeper, hence the impact force from the diamond dresser is transferred deeper into the wheel. For asynchronous dressing, the interference angle is very shallow so the force from the diamond dresser influences a much smaller region of the abrasive wheel. Hence smaller power difference and less fracturing in the wheel, giving a more 'closed' structure with a topography consisting of fewer sharp cutting points (peaks) and lots of dull grains in close proximity.

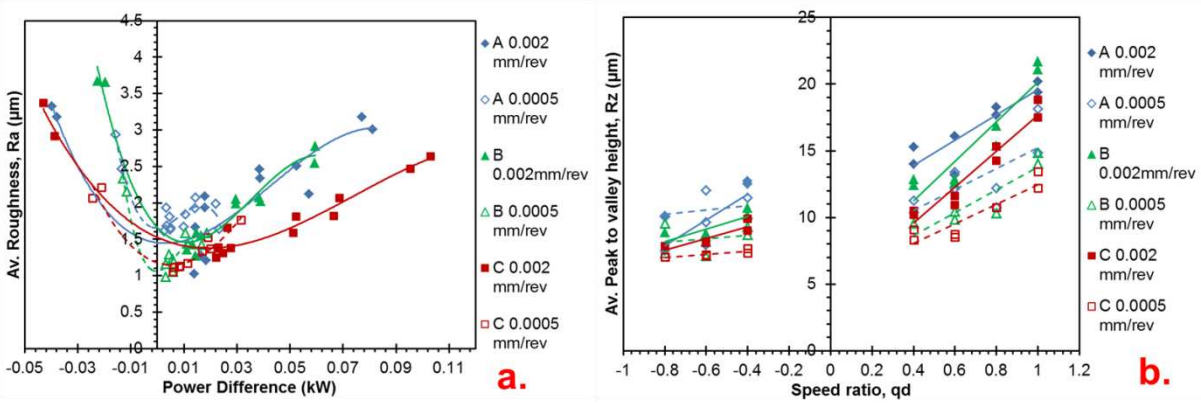

Figure 8 – Average graphite coupon roughness (a) Ra as a function of power difference (b) Rz as a function of speed ratio.

For all wheels, the graph is much steeper at the high infeed rate in Figure 8b suggesting that the higher the infeed rate, the more significant the speed ratio. At low infeed rates the crush dressing effect is reduced so collision forces between the diamonds and the abrasive are lower. This results in decreased fracturing of grains, so less sharp grits are generated to help produce a less rough wheel surface. Also, the Rz values for both infeed rates were lower in asynchronous dressing conditions. This is because the interference angle is closer to the tangent of the wheel [2] causing grains on the surface to shear flat and flattened regions to be generated on the surface of the wheel, hence a reduced surface roughness on the coupon as there is less height variation on the wheel surface.

Although wheel C had the highest power consumption it had the smallest variation in Ra and Rz (Figure 8) between all the wheels. Grit orientation causes the grains not to fracture in the same way during dressing. Assuming only grains in a certain orientation will cut the workpiece, then the roughness of the wheel will be influenced more by abrasive grain ordering compared to the other wheels. As the distribution of grains in vitrified abrasive wheels is random the influence of fractured grains will be reduced by those of an unfavourable orientation. Hence, lower Ra and Rz variation. For conventional grits however, grit morphology is more consistent, hence more uniform grit shapes will be developed on the wheel during dressing so a more aggressive surface generated under more aggressive dressing conditions (high speed ratios, infeed rates). Wheel B showed the most variation in graphite (Ra) roughness, suggesting a possible change in mechanism under different dressing conditions, from micro to macro fracturing of grits.

Peak density was also calculated as it can indicate the fracture mechanism of the wheel. Figure 9a shows that there is a reduction in the peak density for wheel A (at high infeed rate) as the speed ratio approaches unity that could be due to the fracturing of the bond material causing whole grain pull out [27]. For the low infeed rate, the rate of change in peak density with speed ratio is reduced suggesting less bond fracturing because the crush dressing effect is reduced. For wheels B and C a similar decrease in rate of change of peak density was displayed indicating that whole grain pull out is minimal for these wheels. This data is limited as it does not reveal microfracturing because of the data point spacing (see section 2.1) so only whole-grain pull out can be captured.

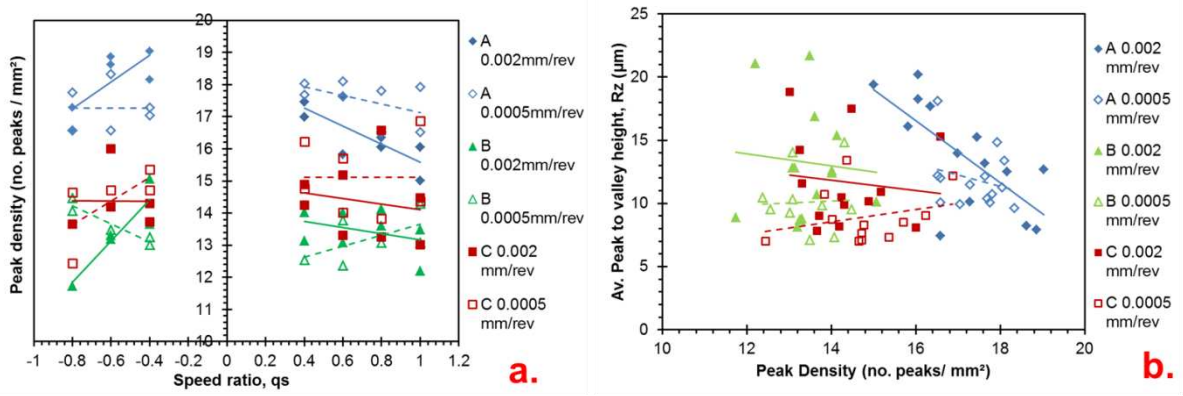

Figure 9 – (a) Peak density of abrasive wheels (b) Graphite coupon Rz as a function of peak density.

Figure 9b shows the variation of the measured Rz of the graphite coupon against peak density. It is clear that for conventional grit shapes (wheel A), under high infeed, high speed ratio conditions there is increased grain pull-out which generates less, but sharper cutting points as there is increased fracturing of both abrasive grain and bond. This is reflected in a higher Rz value at low peak densities. For wheels B and C, this effect is less clear due to the abrasive grains having an engineered morphology so grain orientation influences dressing response. The behaviour of grits is not consistent across the wheel surface during dressing (unlike wheel A) so a trend is less clear.

This is supported by the graph of Figure 10 which shows that at low peak densities, the cutting edges are sharper (lower cumulative frequency gradient, see section 2.1, Figure 3). This is most clear for wheel A but it implies that for any grit morphology, under more aggressive dressing conditions, sharper grits are generated. For the low infeed rate however this trend is not apparent because of the reduced fracture from decreased crushing.

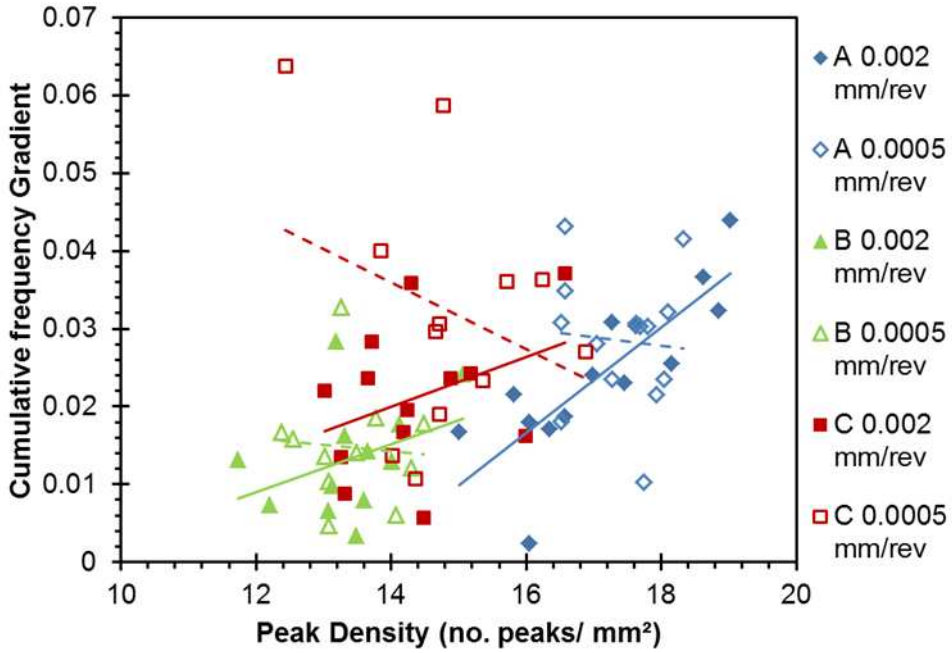

Figure 10 – Gradient of cumulative frequency graph as a function of peak density.

Figure 11 shows the identified 'flat' regions on the obtained optical micrographs of the grinding wheels where the percentage of pixels above the threshold intensity is shown. Across all the wheels, the rate of change of percentage of fracture flats with speed ratio is a very flat trend, therefore the speed ratio has little influence on flat regions generated. For wheel A however there is a noticeable

increase in flat regions generated (0.2%) for the high infeed rate compared to the low. This suggests that because there is increased fracturing overall, it is more likely that flat regions will be generated on the grits. This effect is not seen on wheels B and C. The phenomenon seen in wheel A supports behaviour in Figure 9 (less cutting points at high infeed rate) because more flat regions are produced on the surface causing a reduction in peaks.

For wheels B and C there is no impact of infeed rate and speed ratio on the percentage of fracture flats because of the larger aspect ratio of their grains. Depending on orientation, the surface area of each grit at the wheel surface can vary significantly. Hence changes in orientation dominate any effect on flat regions caused by dressing parameters.

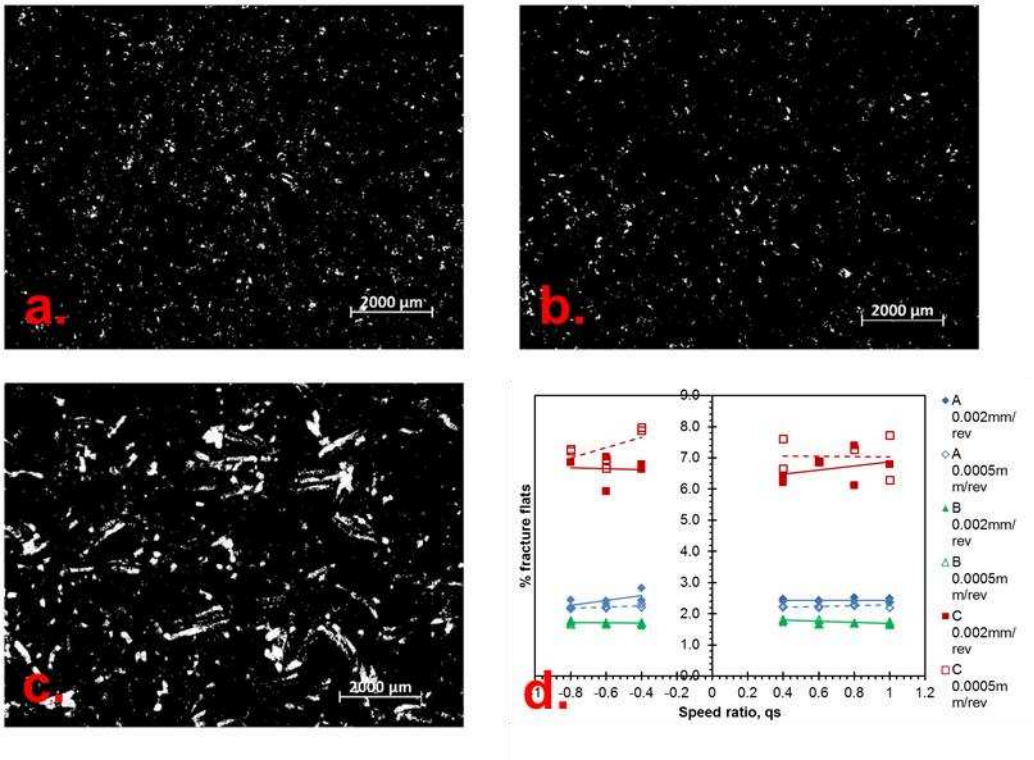

Figure 11 – Fracture flats on the surface of abrasive wheels over the threshold intensity (a) Conventional grit (wheel A) (b) triangular grit (wheel B) (c) elongated grit (wheel C) (d) plot of fracture flats against speed ratio.

It is evident in Figure 11d that wheel C has far more flat regions on the circumference of the wheel. This is also related to abrasive grain orientation as the elongated grains of wheel C can lie flat to the surface (see Figure 11c) creating a large flat area on the surface. Hence this suggests that wheel C has a higher natural quantity of flat regions and they are not strongly influenced by the dressing conditions applied to the wheel.

4.0 Conclusions

This paper investigated the topographical changes that occurred on the surface of three different vitreous-bonded alumina grinding wheels, with different grit morphologies, as a result of different roller dressing parameters. The conclusions that can be drawn are:

- Grit morphology influences dressing response of the grinding wheel. The fracture mechanisms are not consistent between wheels and engineered grit shapes are heavily impacted by grain orientation.
- At high infeed rates and high synchronous speed ratios the power consumption during dressing is high due to increased crush dressing effects and high interference angle.

- High power consumption generates a very coarse wheel with a reduced number of cutting points as higher forces causes increased grain pull out and fracturing.
- When the number of cutting points is reduced, the sharper the active grains for conventional grit shapes.
- Infeed rate has the greatest impact on fracturing of the wheel grits and the higher the rate, the more significant the speed ratio.

Acknowledgements

This research was supported by Rolls-Royce and EPSRC (grant #1503713).

References

[1] W. Rowe, Principles of modern grinding technology, 1st ed. Oxford: William Andrew, 2009.
[2] K. Wegener, H. W. Hoffmeister, B. Karpuschewski, F. Kuster, W. C. Hahmann, and M. Rabiey, "Conditioning and monitoring of grinding wheels," CIRP Ann. - Manuf. Technol., vol. 60, no. 2, pp. 757–777, 2011.
[3] A. Saad, R. Bauer, and A. Warkentin, "Investigation of single-point dressing overlap ratio and diamond-roll dressing interference angle on surface roughness in grinding," Trans. Can. Soc. Mech. Eng., vol. 34, no. 2, pp. 295–308, 2010.
[4] S. Malkin and C. Guo, Grinding Technology: Theory and Application of Machining with Abrasives, 2nd ed. New York: Industrial Press Inc., 2008.
[5] F. Klocke, S. L. Soo, B. Karpuschewski, J. a. Webster, D. Novovic, A. Elfizy, D. a. Axinte, and S. Tönissen, "Abrasive machining of advanced aerospace alloys and composites," CIRP Ann. - Manuf. Technol., vol. 64, no. 2, pp. 581–604, 2015.
[6] X. Chen and W. Rowe, "Analysis and simulation of the grinding process. Part I: generation of the grinding wheel surface," Int. J. Mach. Tool*s* ..., vol. 36, no. 8, pp. 871–882, 1996.
[7] E. Brinksmeier, J. C. Aurich, E. Govekar, C. Heinzel, H.-W. Hoffmeister, F. Klocke, J. Peters, R. Rentsch, D. J. Stephenson, E. Uhlmann, K. Weinert, and M. Wittmann, "Advances in Modeling and Simulation of Grinding Processes," CIRP Ann. - Manuf. Technol., vol. 55, no. 2, pp. 667–696, Jan. 2006.
[8] A. A. Torrance and J. A. Badger, "Relation between the traverse dressing of vitrified grinding wheels and their performance," Int. J. Mach. Tools Manuf., vol. 40, no. 12, pp. 1787–1811, 2000.
[9] S. Malkin and T. Murray, "Mechanics of Rotary Dressing of Grinding Wheels," J. Eng. Ind., vol. 100, no. 1, pp. 95–102, 1978.
[10] B. Linke, "Dressing process model for vitrified bonded grinding wheels," CIRP Ann. - Manuf. Technol., vol. 57, no. 1, pp. 345–348, 2008.
[11] F. Klocke and B. Linke, "Mechanisms in the generation of grinding wheel topography by dressing," Prod. Eng., vol. 2, no. 2, pp. 157–163, 2008.
[12] D. a. Doman, a. Warkentin, and R. Bauer, "A survey of recent grinding wheel topography models," Int. J. Mach. Tools Manuf., vol. 46, no. 3–4, pp. 343–352, 2006.
[13] D. Aslan and E. Budak, "Semi-analytical force model for grinding operations," Procedia CIRP, vol. 14, pp. 7–12, 2014.
[14] W. R. Backer, E. R. Marshall, and M. C. Shaw, "The size effect in Metal cutting," Trans. Asme, vol. 74, no. 1, 1952.
[15] L. a. Blunt and S. Ebdon, "The Application of Three-Dimensional Surface Measurement Techniques to Characterizing Grinding Wheel Topography," *Int. J. Mach. Tools ...*, vol. 36, no. 1, pp. 1207–1226, 1996.
[16] D. Herman and J. Krzos, "Influence of vitrified bond structure on radial wear of cBN grinding

wheels," J. Mater. Process. Technol., vol. 209, no. 14, pp. 5377–5386, 2009.
[17] A. T. Nguyen and D. L. Butler, "Correlation of grinding wheel topography and grinding performance: A study from a viewpoint of three-dimensional surface characterisation," J. Mater. Process. Technol., vol. 208, no. 1–3, pp. 14–23, 2008.
[18] R. Cai and W. B. Rowe, "Assessment of vitrified CBN wheels for precision grinding," Int. J. Mach. Tools Manuf., vol. 44, no. 12–13, pp. 1391–1402, 2004.
[19] D. L. Butler, L. . Blunt, B. . See, J. . Webster, and K. . Stout, "The characterisation of grinding wheels using 3D surface measurement techniques," J. Mater. Process. Technol., vol. 127, no. 2, pp. 234–237, 2002.
[20] S. Lachance, R. Bauer, and A. Warkentin, "Application of region growing method to evaluate the surface condition of grinding wheels," Int. J. Mach. Tools Manuf., vol. 44, no. 7–8, pp. 823–829, 2004.
[21] N. Arunachalam and B. Ramamoorthy, "Texture analysis for grinding wheel wear assessment using machine vision," Proc. Inst. Mech. Eng. Part B J. Eng. Manuf., vol. 221, no. 3, pp. 419–430, 2007.
[22] H. Yasui, Y. Hiraki, and M. Sakata, "Development of automatic image processing system for evaluation of wheel surface condition in ultra-smoothness grinding," Proc. 16th Annu. Meet. ..., 2001.
[23] D. Bhaduri, S. L. Soo, D. Novovic, D. K. Aspinwall, P. Harden, C. Waterhouse, S. Bohr, a. C. Mathieson, and M. Lucas, "Ultrasonic assisted creep feed grinding of Inconel 718," Procedia CIRP, vol. 6, pp. 615–620, 2013.
[24] T. W. Hwang, C. J. Evans, and S. Malkin, "High Speed Grinding of Silicon Nitride With Electroplated Diamond Wheels, Part 1: Wear and Wheel Life," J. Manuf. Sci. Eng., vol. 122, no. 1, p. 42, 2000.
[25] T. W. Hwang, C. J. Evans, and S. Malkin, "High Speed Grinding of Silicon Nitride With Electroplated Diamond Wheels, Part 2: Wheel Topography and Grinding Mechanisms," J. Manuf. Sci. Eng., vol. 122, no. 1, p. 42, 2000.
[26] T. Murray and S. Malkin, "Effects of Rotary Dressing on Grinding Wheel Performance," J. Eng. Ind., vol. 100, no. 3, pp. 297–302, 1978.
[27] M. J. Jackson and B. Mills, "Microscale wear of vitrified abrasive materials," J. Mater. Sci., vol. 39, no. 6, pp. 2131–2143, 2004.